Experimental investigation of effects of airflows on plasma-assisted combustion actuator characteristics*

Liu Xing-Jian(刘兴建)†, He Li-Ming(何立明), Yu Jin-Lu(于锦禄), and Zhang Hua-Lei(张华磊)

Science and Technology on Plasma Dynamics Laboratory, Aeronautics and Astronautics Engineering College, Air Force Engineering University, Xi'an 710038, *China*

(Received 3 September 2014; revised manuscript received 29 October 2014; published online 10 February 2015)

The effects of the airflow on plasma-assisted combustion actuator (PACA) characteristics are studied in detail. The plasma is characterized electrically, as well as optically with a spectrometer. Our results show that the airflow has an obvious influence on the PACA characteristics. The breakdown voltage and vibrational temperature decrease, while the discharge power increases compared with the stationary airflow. The memory effect of metastable state species and the transportation characteristics of charged particles in microdischarge channel are the dominant causes for the variations of the breakdown voltage and discharge power, respectively, and the vibrational temperature calculated in this work can describe the electron energy of the dielectric barrier discharge plasma in PACA. These results offer new perspectives for the use of PACA in plasma-assisted combustion.

Keywords: plasma-assisted combustion actuator, breakdown voltage, discharge power, vibrational temperature

PACS: 51.50.+v, 52.77.–j, 52.70.–m **DOI:** 10.1088/1674-1056/24/4/045101

1. Introduction

Gas discharge occurs in an electrode configuration in which at least one electrode is covered by a dielectric. This discharge in this kind of configuration is called a dielectric barrier discharge (DBD). Sometimes it is referred to as either a silent discharge, since it operates noiselessly,[1] or a corona discharge[2] with a dielectric according to the physics of the process. The very first experiment on a dielectric barrier discharge was reported by Siemens in 1857. Thorough research with new diagnostic techniques and numerical modeling started in the 1970s.[3] The DBD has been extensively used in many different applications, such as ozone generation, decontamination of gas streams, surface treatments, and drag reduction. However, it is only in the last decade that its applications in combustion and aerodynamics have begun to be investigated. New fields, like plasma-assisted combustion (PAC) and airflow control, have emerged.[4,5] The technology of plasma-assisted combustion has many advantages, such as improving the reliability of re-ignition of aero-engines in the sky,[6–8] reducing the ignition delay time of pulse detonation engines (PDE),[9,10] scramjet engines,[11,12] and enhancing the range of stable combustion, promoting combustion completion.[13,14] The plasma-assisted combustion actuator (PACA) is a core component of a plasma-assisted combustion experimental system, and in this paper we study some of the characteristics of a PACA under different airflows.

DBDs have been widely studied in the volume and surface discharge configuration,[15,16] using different working gases, such as He, Ar, N_2, air, and their mixtures, but most of these studies are in stationary conditions. The use of DBD plasmas in low-speed and high-speed airflows has become a recent topic of interest in the field of airflow control.[17] Wang *et al.*[18] studied the effect of a low-speed airflow on the dielectric barrier discharge in ambient atmospheric pressure, showing that the discharge patterns varied from filaments to curved stripes and the discharge intensity decreased when a fast airflow was introduced into the discharge gap. Pavon *et al.*[3] investigated the interaction between high-speed gas flows and surface dielectric barrier discharge, finding that the overall discharge and individual microdischarge (MD) are affected by the surrounding airflow and the geometry of the electrodes has a significant influence on the airflow–plasma interaction. Luo *et al.*[19] studied the effect of the helium flow in a dielectric barrier discharge of atmospheric helium, revealing that the nitrogen molecules as an impurity in helium play a more important role in influencing the behavior of helium discharge than the products created by etching the dielectric surface by discharge.

Up to now, atmospheric pressure volume DBDs in air have been tested, but few of them have been used to enhance combustion performance through injecting ionized airflows into combustor. The plasma-assisted combustion actuator that is designed by us is used in this way, and its characteristics need to be studied. Besides, DBDs in low-speed gas flows have begun to be studied theoretically and numerically,[20,21] but experimental research results are insufficient to analyze these mechanisms and solve their problems.

In the present paper, we focus on the plasma-assisted combustion actuator by using typical electrode arrangements of a cylindrical dielectric barrier discharge and their character-

*Project supported by the National Natural Science Foundation of China (Grant Nos. 51436008, 50776100, and 51106179).

†Corresponding author. E-mail: lxjkgd@163.com

© 2015 Chinese Physical Society and IOP Publishing Ltd

istics under different airflows. The effects of airflows on the breakdown voltage, discharge power, emission spectrum, and plasma vibrational temperature are investigated. The results can be used as a reference for studying the plasma-assisted combustion and its parameter control.

2. Experimental setup

The scheme of experimental setup is represented in Fig. 1(a). The detailed geometry of the plasma-assisted combustion actuator is shown in Fig. 1(b).

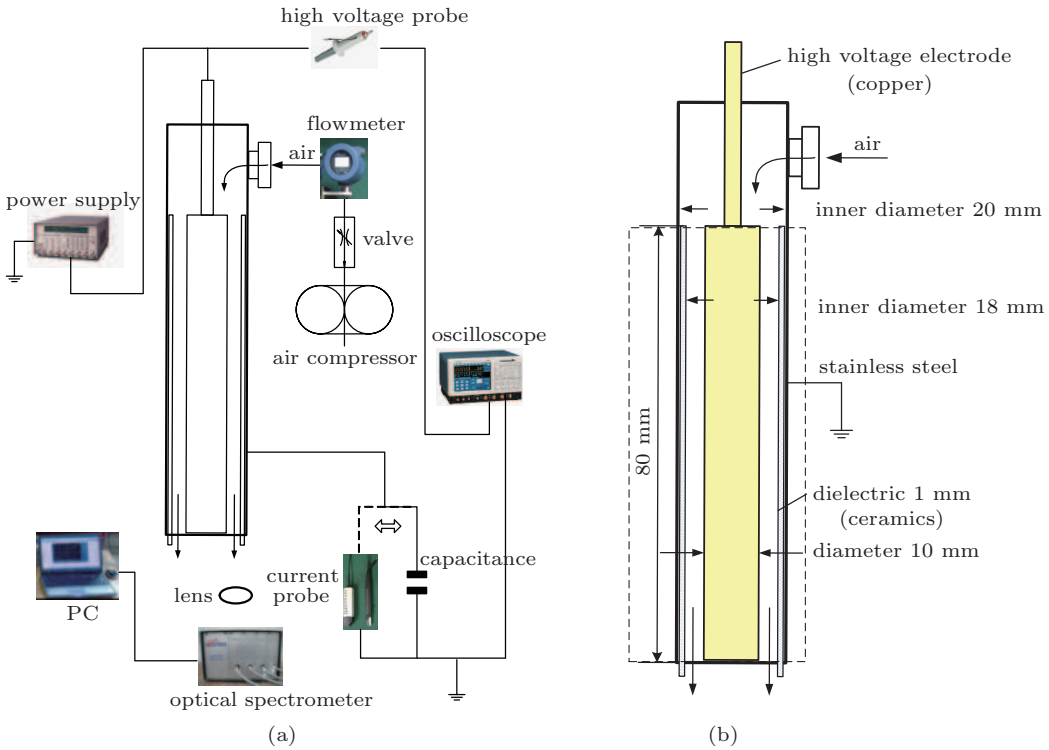


Fig. 1. (color online) (a) Experimental setup and (b) detailed drawings of the PACA geometry.

The actuator can be divided into two parts: the dotted area denotes the gas discharge region, covering an 80-mm length. Typical electrode arrangements of cylindrical dielectric barrier discharge are applied to the PACA. The high voltage electrode in the discharge zone is a 10-mm diameter screw rod that is made of copper. The grounded electrode has a 20-mm inner diameter and is made of stainless steel. The ceramic dielectric tube with a 18-mm inner diameter and 85-mm length is tightly attached to the grounded electrode. So, the discharge gap is 4 mm. The ceramic tube is chosen to be longer in order to avoid creepage at its edges.

The discharge is driven by a sinusoidal power supply with a frequency in a range from 5 kHz to 25 kHz and a maximum peak-to-peak voltage of 30 kV. The diagnostic methods used to study the plasma characteristics are both electrical and optical. The current and voltage on the circuit are measured with current probe (Tektronix, TCP0030) and high voltage probe (Tektronix, P6015A). A capacitor with 0.47 μF in capacitance is connected to measure the charge transfer in order to estimate the discharge power. The signals are sent to a digital oscilloscope (Tektronix, DPO4104B with a band pass frequency of 1 GHz) for display and storage. The emission intensity signals are registered by a multichannel spectrometer (AvaSpec-ULS2048-4-USB2, with a slit width of 10 μm, wavelength of 200 nm∼950 nm, and optical resolution of 0.1 nm∼0.28 nm). An air compressor is used to generate airflow with a valve controlling the airflow rate, and it is then measured by a mass flowmeter (Sincerity, DFM-1-DX).

3. Results and discussion

The addition of airflow to a volume dielectric barrier discharge has a significant effect on the plasma characteristics, which is demonstrated in the following sections by using three different measurements: voltage, current, and emission spectrum. The observations are illustrated at a given frequency of 16.26 kHz, duty cycle of 80%, and effective primary voltage of 93 V.

3.1. Breakdown voltage

Figure 2 shows the breakdown voltage as a function of airflow rate, which is the rms voltage at which plasma forms over the whole discharge zone. The breakdown voltage exhibits complex behavior as the airflow rate increases. As shown in Fig. 2, the whole process can be divided into three stages according to breakdown voltage versus airflow rate: Stage I, Stage II, and Stage III, and the breakdown voltage

monotonically varies in each stage. The results show that the breakdown voltage reaches its maximum value of 5.92 kV at zero airflow and it has a lowest value of 3.24 kV at a certain airflow rate (80.8 g/min). Meanwhile, the breakdown voltage is 5.2 kV with an airflow rate of 160.9 g/min.

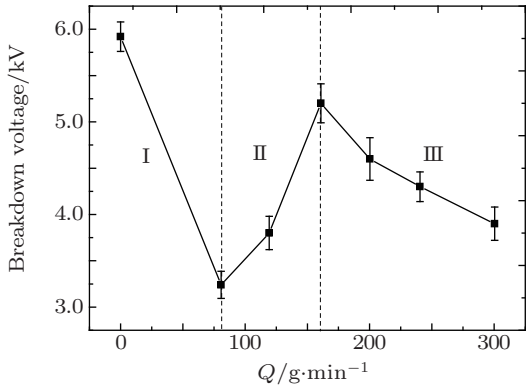


Fig. 2. Discharge breakdown voltage versus airflow rate for the PACA.

As is well known, the memory effect of wall charges is a main factor that affects the DBD in stationary airflow. The discharge characteristics vary when the airflow is introduced into the PACA. It may have four possible factors responsible for this phenomenon: pressure, wall charge, ion velocity, and active particle. Firstly, Sublet *et al.*[22] have studied that for a DBD operated with nitrogen, the pressure must be raised by one order of magnitude to change the breakdown voltage by a factor of two. The pressure level change inside the PACA is less than 30%, which is absolutely too small to account for the variation of the breakdown voltage. Secondly, wall charges can toughly stick to the dielectric through the polarization of the dielectric. It is generally believed that only the recombination with charges of different polarity or γ-emission caused by positive ion bombardment of the dielectric barrier surface can result in the loss of wall charges. Therefore, the loss of wall charges due to the airflows can be ignored. Moreover, the modifications of ion velocity due to airflow are not large enough to explain the phenomenon. The thermal velocity of the electrons is on the order of $\sim 10^6$ m/s, while the thermal velocity of ions is about the velocity of sound that is ~ 300 m/s,[3] which is four orders of magnitude smaller than the thermal velocity of electrons. Finally, because the drift velocities of ions and electrons are much larger than the velocity of airflows, the majority of charged particles move along the direction of electric field. So, the prime factor for the breakdown voltage variation is the active particle.

There are many active particles produced in DBD, involving ions, electrons, excitation states, metastable states, etc. The most possible particle is of metastable state, and a dominant cause for the breakdown voltage variation is the depletion of metastable state, which is purged out from one period of the voltage to the other by the airflow. The lifetime of nitrogen metastable states is on the order of $\sim 10^{-2}$ s, which is much longer than that of any other particle. So, they have enough time to move under the propulsion of airflows. Due to the fact that the electric field introduced by wall charges was not restricted in the MD channel and it is distributed in a certain area, the electric field of wall charges near the metastable state is still very powerful, and the existence of metastable state particles can reduce the breakdown voltage dramatically (it can be called the memory effect of metastable state species), inducing new MDs to emerge, in which place the metastable molecules exist. Indeed, optical emission spectrum measurements in Fig. 3 can exhibit this phenomenon. Figure 3 shows the emission spectra from the DBD plasma for three discharge stages, and the variations of emission spectrum intensities are all in accordance with breakdown voltage modifications.

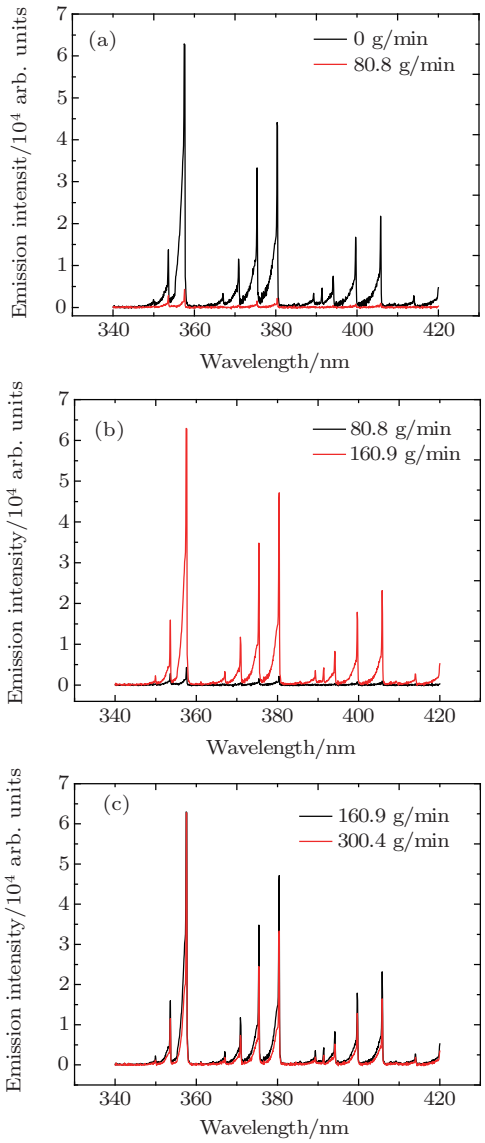


Fig. 3. (color online) Emission spectra from the DBD plasma for three discharge stages, (a) Stage I; (b) Stage II; (c) Stage III.

The main features of the emission spectra are: the N_2 second positive system ($C^3\Pi_u$ to $B^3\Pi_g$ transitions) appears in a range from 300 nm to 500 nm, and the spectra are displayed in a range from 340 nm to 420 nm. When airflow is

introduced into the PACA, the intensity of the emission first decreases in Stage I and then increases in Stage II, and finally becomes weak in Stage III. In other words, the density of metastable molecules experiences a variation process of decreasing–increasing–decreasing. Because the metastable state is the primary factor that affects the breakdown voltage and the existence of metastable molecules can reduce the breakdown voltage dramatically, the breakdown voltage variation has nearly the same trend as the emission intensity. Moreover, due to the distributions of neutrals and metastables have a significant effect on the breakdown mechanism of air dielectric barrier discharge, when the additional airflow is brought into PACA, the breakdown mechanism may have a change. However, as reported in Ref. [18], discharge frequency has an influence on the discharge intensity and discharge mechanisms. There exists a critical frequency separating the discharge mechanisms. When the discharge frequency is above 1 kHz, it is a mode of the streamer discharge, or it is a Townsend discharge. The experimental investigation on PACA is conducted with a fixed frequency 16.26 kHz and maximum airflow speed 15.3 m/s, which is lower than the maximum speed 60 m/s in Ref. [18]. So, it could be inferred that the breakdown mechanism does not change when airflow is added into the PACA, and it always maintains the streamer discharge. In other words, the air photoionization process, which could provide an additional source of electron seed charge, should be considered in the theoretical analysis and numerical simulation.

3.2. Discharge power

The discharge current of ACDBD consists of multiple narrow pulses which are superimposed on the displacement current.[23] The discharge power can be determined by the Lissajous method that was originally proposed by Manley.[24] An additional capacitor with 0.47 μF in capacitance, connected in series with the discharge circuit, is used to accumulate the total charge during one AC half-cycle and its voltage versus the discharge voltage is plotted. The discharge power can then be determined by calculating the area of Lissajous figure. Figure 4 shows the results of discharge power as a function of airflow rates, showing that as the airflow rate increases, the discharge power increases in Stage I and Stage III, while it decreases in Stage II.

The discharge power of ACDBD is determined by charged particles (electrons and ions) in the MD channel. These charged particles will not purge out in the direction of airflow,[25] but the airflow may have an influence on the transportation characteristics of charged particles in the MD channel. Because the voltage, frequency, and duty ratio of the discharge system are fixed, the number of MD channels will not increase when the airflow comes in the discharge cell.[26–32] In other words, the loss of charged particles can be ignored. A detailed investigation of the stripe pattern in flowing argon discharge system[25] has demonstrated that the airflow results in the movement of the discharge filament and its moving velocity increases with the increase of the airflow rate. Moreover, the effects of airflows on MDs can be summarized into the movements of metastable molecules in the direction of airflows and the reduction of diameters of MD channels: the movements of metastable molecules enhance the momentum interchange between charged particles and metastable molecules, slowing down the transportation of charged particles in MD channel and reducing discharge power while diameters of MD channels decrease with the increase of airflow rate, thereby enhancing the efficiency of charged particle transportation and increasing discharge power. The factor that plays a vital role determines the final result. Because the dominant cause varies in different stages, the discharge power fluctuates. In Stage I and Stage III, the transportation of charged particles is sensitive to the reduction of diameters of MD channels, and it is more obvious in Stage III. However, owing to the influence between metastable molecules and charged particles, the transportation of charged particles becomes slow, leading to the decrease of discharge power in Stage II.

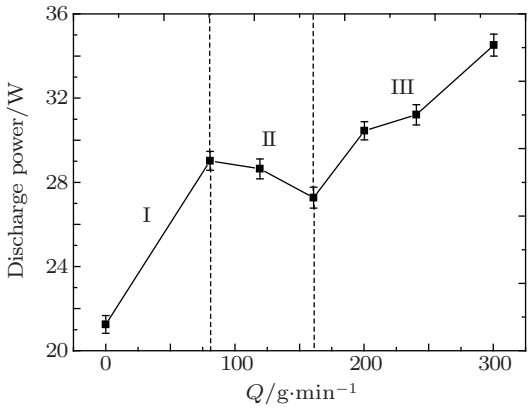


Fig. 4. Discharge power versus airflow rate for the PACA.

3.3. Vibrational temperature

Figure 5 shows the typical emission spectrum of the air plasma of PACA in a range of 200 nm∼950 nm. The predominant part of the emission emitted by the plasma originates from the second positive system (SPS). Additionally, bands with lower intensity from the first negative system (FNS) can be observed. These transitions are well known in the literature. A detailed description of the processes in air plasma is given, for example, in Refs. [33] and [34].

If the plasma is in thermodynamic equilibrium (TE) or in local thermodynamic equilibrium (LTE), the vibrational temperature $T_{\rm vib}$ could be an indicator of the kinetic energy of the molecules. In the present non-equilibrium plasma of DBD, the vibrational temperature $T_{\rm vib}$ is obtained instead. It can be determined by a Boltzmann plot.[35] The intensities of bands from different vibrational transitions are determined and

$\ln(I_{v'v''}/\nu_{v'v''}A_{v'v''})$ against $E_{v'}$ is plotted. The points lie on a straight line with a slope of $-1/kT_{\rm vib}$, and $T_{\rm vib}$ can be calculated. Although $T_{\rm vib}$ is neither equal to the electron temperature nor the rotational temperature, it follows some trend and gives useful information about excitation and de-excitation in the system, especially the electron energy. Optical emission spectra in a range of 340 nm∼440 nm under different airflow rates are plotted in Fig. 6, and three vibrational bands of the SPS are used to calculate the vibrational temperature: $\Delta v = -1$ (0–1, 1–2, 2–3), $\Delta v = -2$ (0–2, 1–3, 2–4), $\Delta v = -3$ (0–3, 1–4, 2–5).

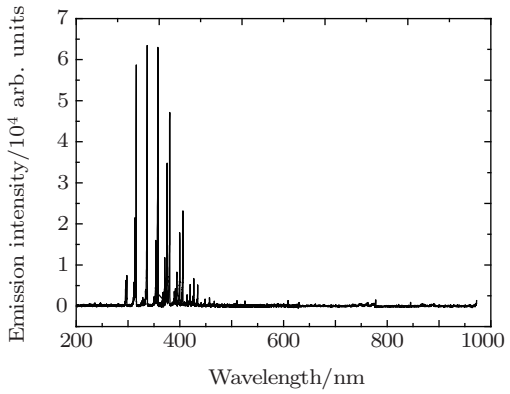


Fig. 5. Characteristic emission spectrum in a range of 200 nm–950 nm.

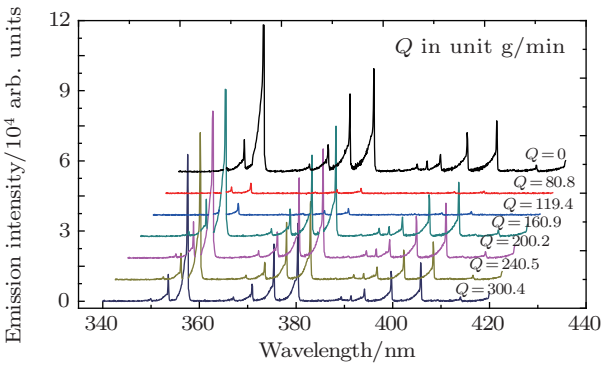


Fig. 6. (color online) The optical emission spectra in a range of 340 nm∼440 nm under different airflow rates.

Figure 7 displays the vibrational temperature in the plasma. Without airflow, the vibrational temperature amounts to 3657 K and decreases significantly with increasing the airflow. The electrons obtain a great deal of energy from electric field and impact on nitrogen. As long as the electron energy is lower than ionization energy of nitrogen molecule, the impact would only lead to nitrogen molecule excitation and elastic impact. The higher the electron energy, the more highly the nitrogen molecules are excited, and the higher the vibrational temperature will be. If the ionization of nitrogen molecule occurs, it will produce a large number of N_2^+ ions, and this process could result in the decrease of vibrational temperature. However, there is no apparent spectral line of $\lambda = 391.4$ nm. On the one hand, it illustrates that electron energy gained from electric field is mostly lower than the ionization energy in the discharge system of the PACA. On the other hand, the vibrational temperature calculated in this work can describe electron energy.

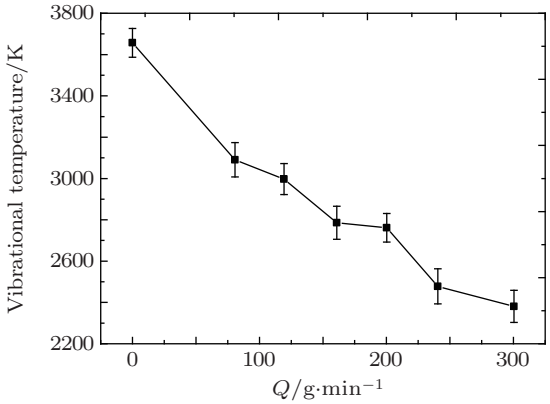


Fig. 7. Vibrational temperature versus airflow rate for the PACA.

4. Conclusions

In the present work, the effects of the airflows on plasma-assisted combustion actuator characteristics are investigated. The characteristics are demonstrated by breakdown voltage, discharge power, and vibrational temperature. The optical emission spectrum measurements show that there are some modifications to the concentration of active particles when airflow is introduced into the plasma-assisted combustion actuator. The memory effect of metastable state species is the primary cause that affects the breakdown voltage in airflow, and there is no change in the breakdown mechanism: a streamer discharge is still maintained. The airflow has an influence on the transportation characteristics of charged particles in the MD channel, resulting in the change of discharge power. Electron energy gained from electric field is mostly lower than ionization energy in discharge system of PACA, and the vibrational temperature calculated in this work can describe electron energy of DBD plasma in PACA. Without airflow, the breakdown voltage and vibrational temperature reach their maximum values, but the discharge power becomes lowest.

References

[1] Ulrich K 2003 *Plasma Chem. Plasma P* **23** 3
[2] Chen J and Davidson J H 2002 *Plasma Chem. Plasma P* **22** 495
[3] Pavon S, Dorier J L, Hollenstein Ch, Ott P and Leyland P 2007 *J. Phys. D: Appl. Phys.* **40** 1733
[4] Igor Matveev and Svetlana Matveeva 2005 43*rd AIAA Aerospace Sciences Meeting and Exhibit*, January 10–13, 2005, Reno, Nevada, USA, p. 1191
[5] Lord W K, MacMartin D G and Tillman T G 2000 *Fluids* 2000, June 19–22, 2000, Denver, USA, p. 2234
[6] Lan Y D, He L M, Ding W and Wang F 2010 *Acta Phys. Sin.* **59** 2617 (in Chinese)
[7] Yu J L, He L M, Ding W, Wang Y Q and Du C 2013 *Chin. Phys. B* **22** 055201
[8] Zhao B B, He L M, Shen Y, Bai X F and Yu J L 2013 *Spectrosc. Spectral Anal.* **33** 1171 (in Chinese)

[9] Wang F, Jiang C, Kuthi A and Gundersen M A 2004 42*nd AIAA Aerospace Sciences Meeting and Exhibit*, March 12–14, 2004, Reno, Nevada, USA, p. 834

[10] Cathey C, Wang F, Tang T, Kuthi A, Gundersen M, Sinibaldi J, Brophy C, Barbour E, Hanson R, Hoke J, Schauer F, Corrigan J and Yu J 2007 45*th AIAA Aerospace Sciences Meeting and Exhibit*, January 8–11, 2007, Reno, Nevada, USA, p. 443

[11] Mozingo J A 2004 "Evaluation of a Strut-Plasma Torch Combination as a Supersonic Igniter-Flameholder", Ph. D. Dissertation (Virginia: Virginia Polytechnic Institute and State University)

[12] Sergey L, Dmitry Y and Campbell C 2009 *J. Propulsion Power* **25** 289

[13] Charles D, Cathey C and Tang T 2007 *IEEE Trans. Plasma Sci.* **35** 1664

[14] Liu J B, Ronney P Wang F, Kuthi A and Gundersen M 2003 41*st AIAA Aerospace Sciences Meeting and Exhibit*, January 6–9, 2003, Reno, Nevada, USA, p. 877

[15] Becker K H 2005 *Non-equilibrium Air Plasmas at Atmospheric Pressure* (Series in Plasma Physics) (Bristol: Institute of Physics Publishing) p. 243

[16] Gherardi N and Massines F 2001 *IEEE Trans. Plasma Sci.* **29** 536

[17] Forte M, Léger L, Pons J, Moreau E and Touchard G 2005 *J. Electrostat.* **64** 215

[18] Wang Z, Ren C S, Nie Q Y and Wang D Z 2009 *Plasma Sci. Technol.* **11** 177

[19] Luo H Y, Liang Z, Wang X X, Guan Z C and Wang L M 2008 *J. Phys. D: Appl. Phys.* **41** 205205

[20] Enloe C L, McLaughlin T E, VanDyken R D, Kachner K D, Jumper E J, Corke T C, Post M and Haddad O 2004 *AIAA J.* **42** 595

[21] Boeuf J P and Pitchford L C 2005 *J. Appl. Phys.* **97** 103307

[22] Sublet A, Ding C, Dorier J L, Hollenstein Ch, Fayet P and Coursimault F 2006 *Plasma Sources Sci. Technol.* **15** 627

[23] Wagner H E, Brandenburga R, Kozlovb K V, Sonnenfeldc A, Michela P and Behnke J F 2003 *Vacuum* **71** 417

[24] Manley T C 1943 *Trans. Electrochem. Soc.* **84** 127

[25] Li X C, Liu R F, Jia P Y and Kong L Q 2012 *Acta Phys. Sin.* **61** 115205 (in Chinese)

[26] Pashaie B, Sankaranarayanan R and Dhali S K 1999 *IEEE Trans. Plasma Sci.* **27** 22

[27] Xudong "Peter" Xua and Mark J K 1998 *J. Appl. Phys.* **84** 4153

[28] Chirokov A, Gutsol A, Fridman A, Sieber K, Grace J and Robinson K 2005 *IEEE Trans. Plasma Sci.* **33** 300

[29] Wagner H E, Yurgelenas Yu V and Brandenburg R 2005 *Plasma Phys. Control Fusion* **47** B641

[30] Nagorny V P 2007 *J. Appl. Phys.* **101** 023302

[31] Luo H Y, Ran J X and Wang X X 2012 *High Volt. Engin.* **38** 1661 (in Chinese)

[32] Liang Z, Guan Z C, Wang L M, Luo H Y and Wang X X 2010 *Acta Phys. Sin.* **59** 8739 (in Chinese)

[33] Zhu Y F, Jia M, Cui W, Ling Y H and Wu Y 2013 *High Volt. Engin.* **39** 1716 (in Chinese)

[34] Starikovskiy A and Aleksandrov N 2013 *Prog. Energy Combust. Sci.* **39** 61

[35] Li X C, Liu R F, Chang Y Y and Zhao H H 2013 *Spectrosc. Spectral Anal.* **33** 308 (in Chinese)